Compression of Fibrous Assemblies: Revisiting the Stress-Density Relation

Catalin R. Picu¹

Department of Mechanical, Aerospace and Nuclear Engineering, Rensselaer Polytechnic Institute, Troy, NY 12180 e-mail: picuc@rpi.edu

Vineet Negi

Department of Mechanical, Aerospace and Nuclear Engineering, Rensselaer Polytechnic Institute, Troy, NY 12180 e-mail: vineetnegi.ism@gmail.com Many engineering materials are made from fibers, and fibrous assemblies are often compacted during the fabrication process. Compression leads to the formation of contacts between fibers, and this causes stiffening. The relation between the uniaxial stress, S, and the volume fraction of fibers, φ , is of power law form. The derivation of this relation based on micromechanics considerations takes as input the structural evolution represented by the dependence of the mean segment length of the network, l_c , on the current density, ρ (ρ is defined as the total length of fiber per unit volume of the network). In this work, we revisit this problem while considering that the mean segment length should be defined exclusively by fiber contacts that transmit load. We use numerical simulations of the compression of crimped fiber assemblies to show that, when using this definition, $\rho \sim 1/l_c^2$ at large enough strains. Purely geometric considerations require that $\rho \sim 1/l_c$, and we observe that this applies in the early stages of compaction. In pre-stressed networks, the densitymean segment length scaling is of the form $\rho \sim 1/l_c^2$ at all strains. This has implications for the relation between stress and the fiber volume fraction. For both ρ versus l_c scalings, $S \sim (\varphi^n - \varphi_0^n)$, where φ_0 is the initial or reference fiber volume fraction; however, n=3 when $\rho \sim 1/l_c$ and n=2 for $\rho \sim 1/l_c^2$. These predictions are compared with experimental data from the literature. [DOI: 10.1115/1.4056180]

Keywords: constitutive modeling of materials, elasticity, micromechanics

1 Introduction

Network materials (materials with structure formed by a network of filaments) are ubiquitous in biology and engineering. Generally, they perform a mechanical role, and their mechanical behavior is dictated by the structure of the underlying network, its evolution during deformation, the properties of filaments, and their contacts or/and crosslinks. Extensive work has been performed to date on defining the relationship between global mechanical behavior and the network structure—see Ref. [1] for a review.

Virtually all network materials have stochastic structure: filaments are distributed randomly and are generally crimped, and filament segments may be either randomly oriented or may exhibit preferential orientation. The structure is characterized with several parameters such as the density (the total length of filaments per unit volume of the network), ρ , filament cross-sectional dimensions (the diameter, d, for cylindrical filaments), and a measure of the preferential orientation (e.g., the orientation tensor). The filament volume fraction can be written as $\varphi = \rho A_f$, where A_f is the cross-sectional area of filaments. Crosslinks and contacts divide fibers in segments. The segment length is exponentially distributed and the mean, l_c , is the only parameter of the distribution [2]. The crosslink/contact density may be written as $\rho_x = \rho l l_c$. l_c also controls the size of pores and hence is a critical parameter for mass transport through the network.

While the mean density, ρ , depends on the total volume occupied by the network, l_c is a microscale parameter that depends on the rate of contact formation during deformation or network generation. The relationship between these two parameters is of central importance in all micromechanical models aimed at predicting material behavior based on the network structure.

Contributed by the Applied Mechanics Division of ASME for publication in the Journal of Applied Mechanics. Manuscript received October 27, 2022; final manuscript received November 1, 2022; published online November 18, 2022. Assoc. Editor: Pradeep Sharma.

The ρ versus l_c relation was inferred based on geometric considerations by evaluating the probability of overlap as fibers are added to a predefined volume (in 3D) or area (in 2D). For 2D planar stochastic distributions of lines of zero width (the Mikado model), the Kallmes–Corte relation indicates that $\rho l_c = 2/\pi$ [2]. This relation remains valid if fibers are not straight [3]. If fibers have finite width, pairs of filaments overlap over a finite area. If the segment length is evaluated based on the intersection of centerlines, the situation becomes identical to that of the Kallmes–Corte model and l_c is independent of the fiber width. An alternative formulation based on the notion of "coverage," which represents the expected number of fibers covering a point in the 2D projection of the network, was developed for paper [4]. Measurements reported in various articles provide support for the relation $\rho_{2D} \sim 1/l_c$, where ρ_{2D} is the density in the 2D projection of the network.

In 3D, the probability of intersection of straight or curved lines (zero thickness fibers) vanishes, and hence, the cross-sectional dimensions must be accounted for. An analysis similar to that of the Kallmes–Corte model leads to the relation $\rho dl_c = 2/\pi$ [5,6]. If fibers are preferentially aligned, the relation $\rho dl_c = \text{const}$ remains valid, with the provision that the constant becomes a function of the degree of alignment [7,8]. The arguments presented for both 2D and 3D networks are based on the evaluation of the volume surrounding a representative fiber that needs to be penetrated by another fiber for a contact or crosslink to be established. This volume depends exclusively on the fiber length and diameter and is independent of the fiber shape. Consequently, the relation $\rho dl_c = \text{const}$ also applies in the case of tortuous filaments [9,10].

However, if filaments have fractal shape, as in molecular networks, the end–end distance of a network segment, l_{ee} , is related to the contour length, l, as $l_{ee} \sim l^{\chi}$, where $1/\chi$ is the fractal dimension of the filament. Hence, the mean end-to-end segment length, referred to as the "mesh size," ξ , is related to l_c (which here means the contour segment length) as $\xi \sim l_c^{\chi}$. A geometric derivation [11] leads to $\rho \xi^{(3\chi-1)\chi} = \text{const}$ or, equivalently, $\rho l_c^{3\chi-1} = \text{const}$. If the network is embedded in a good solvent, case in which the chains are swelled relative to the ideal chain statistics,

¹Corresponding author.

the Flory theory predicts $\chi=3/5$ (also confirmed by experiment [12]), which implies that $\rho \xi^{4/3}={\rm const.}$ i.e., $\rho l_c^{4/5}={\rm const.}$ In semiflexible networks in which the persistence length is large compared to the segment length, segments are not fractal, $\chi=1$, and the ρ versus l_c relation becomes $\rho l_c^2={\rm const.}$

It is useful to note that, if l_c is the only length parameter of the problem (i.e., the filament cross-sectional dimensions are negligible, such as in the case of molecular networks), dimensional analysis requires $\rho l_c^2 = \text{const}$ in 3D.

To summarize, geometric and dimensional considerations lead to either a relation of the type $\rho l_c^2 = \text{const}$ or to $\rho dl_c = \text{const}$ for 3D networks in which the filament diameter may or may not be neglected, respectively. The validity of these relations is re-evaluated in this work.

These relations are central to micromechanical models of athermal network deformation and to poroelasticity. Networks subjected to compression strain stiffen continuously once the density becomes larger than the stiffness percolation density, ρ_p . The stress (uniaxial, in direction of compression) is observed to scale as $S \sim \rho^n - \rho_p^n$, where the value of the exponent n increases as the degree of compaction increases. The model proposed by van Wyk [13], which refers to stochastic assemblies of fibers with random orientation in 3D, predicts n=3. The model is based on the assumption that $\rho dl_c = \text{const.}$ The model proposed by Toll [14,15], which applies to preferentially oriented fibers, predicts an exponent of n=5.

Here, we observe that contacts between filaments are not mechanically relevant unless they transmit loads. This implies that some of the contacts present in an unloaded fiber assembly and identified by the purely geometric procedure leading to the relation $\rho dl_c = {\rm const}$ do not contribute to stress production once the network is loaded. Part of the initial contacts open during loading and new ones are created. Since l_c must be evaluated counting only load bearing contacts, numerical models are used to capture the evolution of the structure. In Sec. 3.1, we present numerical data for the ρ versus l_c scaling, which indicates that the geometric relation $\rho dl_c = {\rm const}$ applies during the initial stages of compression of a filament assembly, after which $\rho l_c^2 = {\rm const}$ holds. In Sec. 3.2, we discuss the implications of this observation for the stress–density relation and compare the experimental data from the literature with the present model.

The density-mean segment length relation captures an essential aspect of structural evolution during deformation and is used in various applications ranging from gels of semiflexible molecules to nonwovens and textiles. In some cases, it is postulated that $\rho l_c^2 = \text{const}$ holds, while in others, $\rho l_c d = \text{const}$ is considered to be valid. This article aims to unify these views by showing that both relations apply, although in different ranges of deformation. The density-mean segment length relation also applies to problems beyond the mechanics of stochastic networks: to poroelasticity and to transport across network materials (filtration).

2 Methods and Models

The models considered here represent the compaction of fiber wads. Fiber centerlines are generated in a domain of dimensions $L \times L \times H$ as angularly restricted random walks (worm-like models) with finite persistence length, L_P .

Each fiber begins at a randomly selected point on the lateral walls of the model and is constructed as a random walk of step-length l_s and in which the orientation of a new segment relative to the preceding one is sampled from a predefined probability distribution specified in the literature for worm-like polymer chain models [16]. The directional correlation of the fiber tangent is characterized by $\langle \cos \theta'(s) \rangle$, where $\theta'(s)$ is the angle between the tangent versors at two points along a given fiber separated by the contour length s. $\langle \rangle$ indicates averaging over multiple fibers and reference points along the given fiber. The directional correlation function is approximated with an exponential, $\langle \cos \theta'(s) \rangle \approx \exp(-s/L_P)$, from where the length parameter, L_P , is obtained. To ensure that a representative

fiber mass is generated, L is equal to $5L_P$. The total fiber length in a model is $\sim 1500L_P$.

Fibers are considered athermal, linear elastic of Youngs modulus E_f and of circular cross section of diameter d. The fiber diameter is taken as the unit of length and is used to normalize all other lengths of the problem. In all subsequent steps, fibers are not allowed to cross and contacts develop as the density increases. Interfiber contacts are modeled as frictionless with Hertz type contact behavior. The length of a segment is evaluated as the contour length between two successive contacts that transmit load.

The fiber assembly is compressed using two punches, as shown in Fig. 1(a) by the red horizontal lines, to a state of density ρ_0 , Fig. 1(b), considered as the reference state. The lateral walls and the punches are impenetrable for fibers during the compression process. Further, two situations are considered: (i) the system is further compacted to density $\rho > \rho_0$; this situation is referred to here as "unrelaxed," and (ii) the strain energy in the state of density ρ_0 is removed and the system is further compacted to density $\rho > \rho_0$; this situation is referred to here as "relaxed." In case (i), most of the contacts present in the reference state carry load, while in case (ii), no such contact carries load.

Fibers are meshed with 3D linear Timoshenko beam elements with element length l_s . Furthermore, the ratio of the element length to the fiber diameter is fixed at $5: l_s/d = 5$. Nonlinear quasistatic explicit method in FEA software ABAQUS 6.14 is used for the analysis. The contacts between the fibers are modeled using the penalty method in the explicit simulations. Normal stress in the compaction direction, S, is measured as the total force per unit initial area (nominal stress). During compaction, impenetrable lateral walls ensure that the area density of fibers remain constant. This would be the case if the region modeled is a representative volume elements (RVE) of a fiber network that extends indefinitely in the directions orthogonal to the loading direction. Three realizations are considered for each case.

3 Results

3.1 Density–Mean Segment Length Relation in Compressed Fiber Assemblies. Figure 2 shows the variation of the mean segment length during compression. The curves labeled by circle and triangle symbols correspond to compression from the unrelaxed and relaxed reference state, respectively, with $\rho_0 d^2 = 2.93 \times 10^{-3}$ for both initial states. The curve shown in green (stars) corresponds to compaction from the relaxed state with $\rho_0 d^2 = 5.86 \times 10^{-3}$.

The unrelaxed network curve has slope -0.5, which implies that for the entire deformation history $\rho l_c^2 = {\rm const.}$ In the relaxed cases, l_c diverges when $\rho \to \rho_0$ since in the reference relaxed case no contact carries load. In these systems, l_c decreases fast at the beginning of the deformation and reaches an intermediate regime in which the slope of the curve shown in Fig. 2 is -1, and hence, $\rho dl_c = {\rm const.}$ The -0.5 slope emerges again at larger degrees of compactions and $\rho l_c^2 = {\rm const.}$ in this regime. As expected, the relaxed systems behave like the unrelaxed networks at large enough compression. Modifying the density of the reference state, ρ_0 , changes the position of the asymptote, but the two regimes described persist.

Figure 2 suggests that at the beginning of the compaction process of a fiber assembly without residual contact stresses, the rate of contact formation depends solely on the fiber diameter, d, and the rate of increase of the density, ρ ; and the higher the excluded volume as a fraction of the total volume, the higher the probability of fiber interaction on a purely geometrical basis. However, once contact forces build up and the internal load sharing structure develops, the rate of contact formation depends on the nonaffinity of the fiber assembly deformation. Since, the nonaffinity of the deformation field decreases with deceasing l_c ; l_c replaces d as an internal length-scale parameter controlling the contact formation rate. Thus, the transition from d dependence to l_c dependence of the

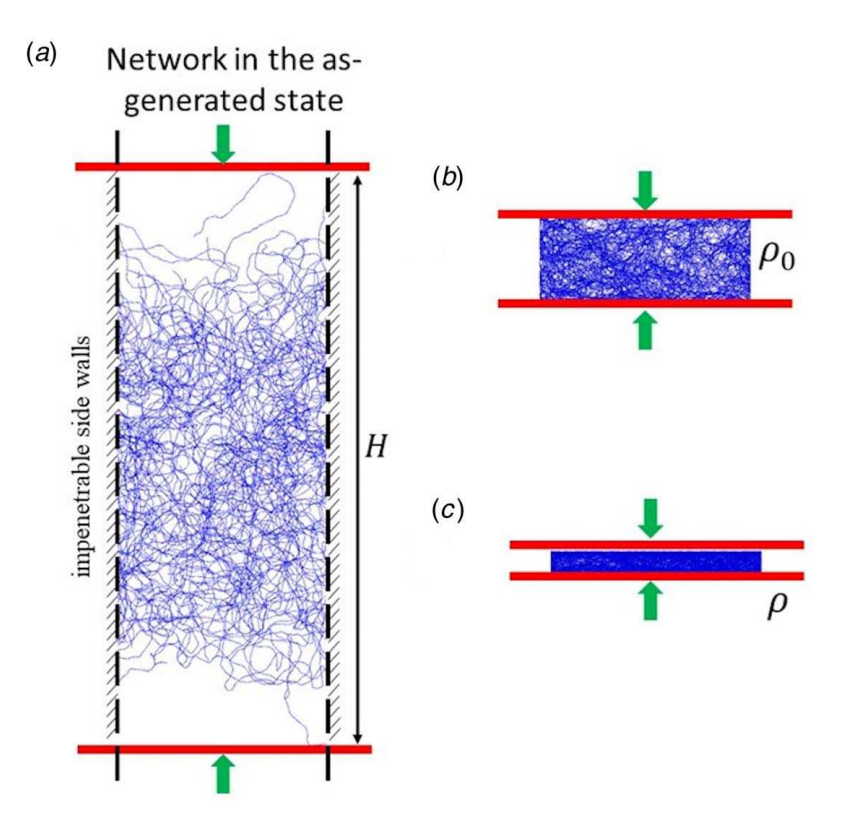


Fig. 1 (a) Network of tortuous fibers generated in a domain of size $L \times L \times H$, (b) reference state of the network of density ρ_0 , and (c) current state of variable density ρ

rate of contact formation emerges from a transition from purely geometric interference-driven contact formation to deformation nonaffinity-driven contact formation.

3.2 Stress–Density Constitutive Relation. These observations may be related to the stress required to compress the fibrous

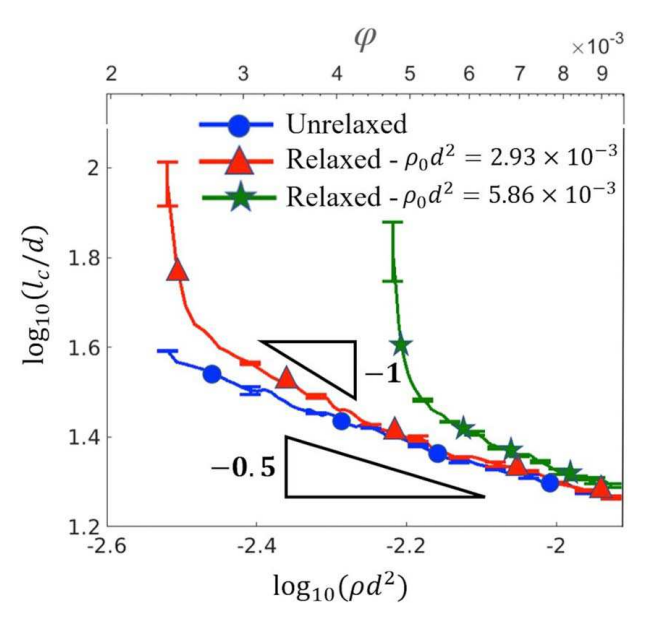


Fig. 2 Variation of the mean segment length, I_c , with the density, ρ , during compression of unrelaxed networks with $\rho_0 d^2 = 2.93 \times 10^{-3}$ (circle symbols) and relaxed network with $\rho_0 d^2 = 2.93 \times 10^{-3}$ (triangle symbols) and $\rho_0 d^2 = 5.86 \times 10^{-3}$ (star symbols). The bars represent standard error of three realizations.

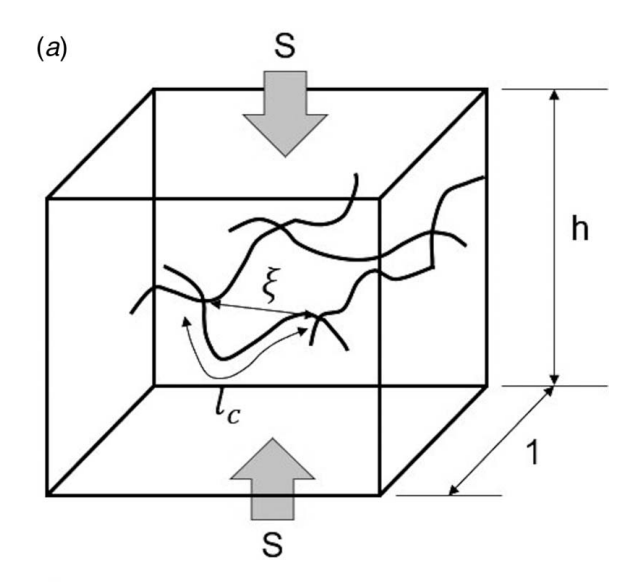
assembly. van Wyk's model [13], which applies to networks with random orientation of fibers, is based on the assumption that the geometric relation ρdl_c = const applies. We revisit the derivation of the stress-density relation and explore its functional form mandated by using the alternative relationship ρl_c^2 = const.

Consider a subdomain of the network as shown in Fig. 3(a), with the mesh size ξ and the mean segment length shown schematically. Based on the definition used here, all contacts shown carry loads. The macroscale stress, S, is associated with these contact forces. P represents the mean contact force in the macroscale loading direction. The mean field incremental relation between S and P can be written as $dS \sim dP/\xi^2$. The associated deformation at the individual fiber scale is computed using the model of Fig. 3(b), where a crimped fiber is simply supported and is loaded by adjacent fibers. The incremental small deflection dy is evaluated assuming elastic deformation as follows:

$$dP \sim (E_f I_f / \xi^2 l_c) dy \tag{1}$$

This expression is similar to that corresponding to a simply supported straight elastic beam, except that here both length scales of the problem, ξ and l_c , are accounted for. It results by observing that if the fibers were straight, Eq. (1) would read $dP \sim (E_f I_f/\xi^3) dy$. However, the bending stiffness of a crimped beam is approximately equal to the bending stiffness of the straight beam of same end-to-end length multiplied by the crimp parameter, ξ/l_c [1]. This may be inferred by observing that the bending moment reduced to an arbitrary point along the fiber scales linearly with ξ , and hence, the strain energy per unit fiber length at the respective site is proportional to ξ^2 . Further, the total strain energy in the crimped fiber scales with $l_c\xi^2$. Castigliano's second theorem indicates that the compliance of the beam should be also proportional to $l_c\xi^2$, which leads to the relation indicated earlier.

To make progress, and following van Wyk's derivation, we make the affine assumption, which requires that the local strain is identical



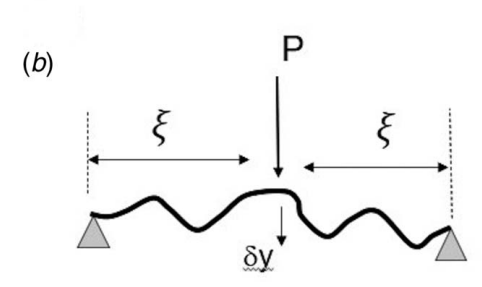


Fig. 3 Schematic used to derive the stress-density relation

to the global strain: $dy/\xi = dh/h$. Further, by using the definition of density and considering the deformation to be axial, it results that $dh/h = -d\rho/\rho$, and therefore,

$$dy = (\xi/h)dh \tag{2}$$

The density of contacts is, by definition, $\rho_x = 1/\xi^3$ and, considering that $\rho_x = \rho/l_c$, one obtains $\xi = (l_c/\rho)^{1/3}$. With this expression for ξ and using Eqs. (1) and (2), the stress increment may be written as follows:

$$dS \sim -(E_f I_f / l_c^2) d\rho \tag{3}$$

The density-mean segment length relation is required at this stage to allow the integration of Eq. (3). By using the geometric relation $\rho dl_c = \text{const}$ to write l_c in terms of ρ , Eq. (3) leads to:

$$S(\rho) \sim E_f I_f(\rho^3 - \rho_0^3) \tag{4}$$

This is the stress–density relation predicted by van Wyk's model. On the other hand, using $\rho l_c^2 = \text{const leads to the relation:}$

$$S(\rho) \sim E_f I_f (\rho^2 - \rho_0^2) \tag{5}$$

The results shown in Fig. 2 suggest that the stress measured during compression in relaxed structures should exhibit two regimes: an early regime in which Eq. (4) applies, followed by a regime in which Eq. (5) applies. Equation (5) is expected to be a good representation of the stress–density relation for the entire deformation in unrelaxed cases. This is indeed seen in simulations. Figure 4 shows the variation of the stress (normalized as S/E_f) versus the density for both unrelaxed and relaxed networks.

3.3 Comparison With Experimental Data and Discussion. Figure 5 shows experimental data from Refs. [17,18] obtained from uniaxial compression of fiber masses in a cylindrical container with

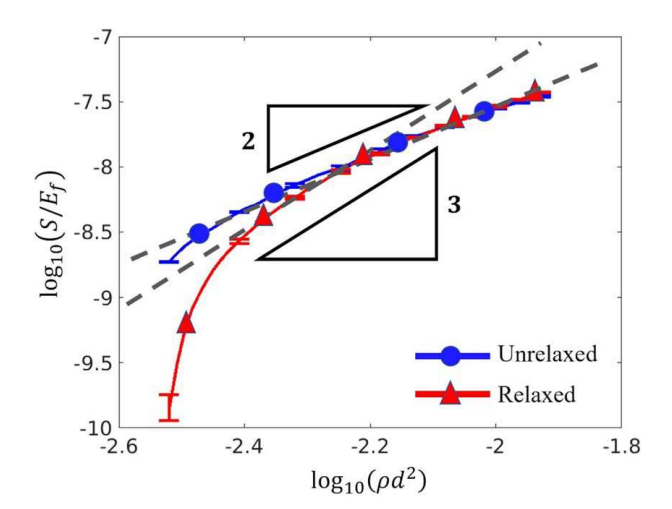


Fig. 4 Nominal stress-density relation during compaction of fibrous assemblies starting from unrelaxed (circle symbols) and relaxed (triangle symbols) states of initial density $\rho_0 d^2 = 2.93 \times 10^{-3}$. The bars represent standard error of three realizations.

hard walls—a geometry similar to that considered in the present models. Data for glass wool, glass yarn, and carbon fiber wool are shown. The horizontal axis represents the mass density normalized with the initial mass density, which is shown in the figure. The mass density is linearly related to the density used here as $\rho_m = \rho \rho_f \pi d^2/4$, where ρ_f is the mass density of the fiber material. The data show the two regimes discussed here: an initial regime in which $S \sim (\rho/\rho_0)^3$, followed at higher densities by a regime with $S \sim (\rho/\rho_0)^2$. The degree of compaction in these experiments is not high enough to produce strong preferential alignment, which would entail an exponent close to 5, as suggested by Toll's model [14] and observed in dedicated experiments [19]. Another data set obtained by compressing cotton, polyester, and wool fiber masses, which covers a broader range of densities, is provided in Refs. [20,21].

Other simulations of network compression [22–26] provide additional support for the present discussion. Durville [25] modeled the compression of noncrosslinked tortuous fiber wads and observed regimes described by exponents 3, 2, and 5 as the fiber volume fraction increases. The transition from the regime characterized by exponent 3 to that characterized by exponent 2 was also observed in Ref. [23] in noncrosslinked networks of initially straight fibers subjected to triaxial compression. The simulation data in [23] and

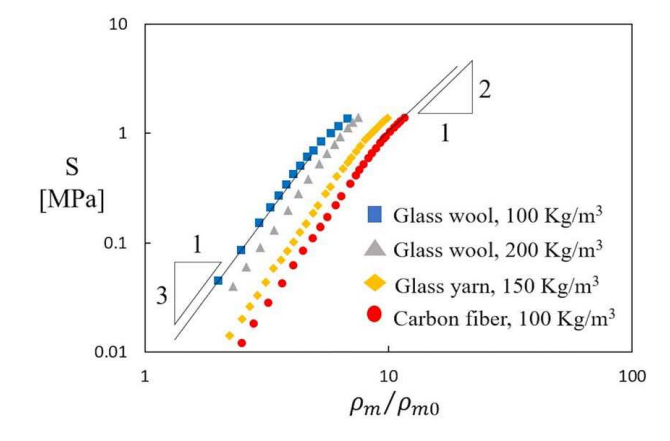


Fig. 5 Experimental stress versus mass density for several types of noncrosslinked networks from Refs. [17,18]. The horizontal axis shows mass density normalized with the initial mass density.

the experimental data in [27] emphasize the importance of preconditioning for the emergence of the regimes discussed here: the regimes become visible after several loading–unloading cycles, while the first cycle exhibits a different behavior. Interfiber friction does not appear to modify this behavior [23,24] although the results presented in Ref. [22] seem to suggest the opposite conclusion.

4 Conclusions

In this study, we perform numerical simulations of the compression of athermal fiber assemblies and evaluate the relationship between density and mean segment length of the network. We observe that the relation $\rho dl_c = \text{const}$, which emerges from geometric considerations, applies only at the beginning of the compaction process, and it is replaced by $\rho l_c^2 = \text{const}$ at later stages. This has implications for the scaling of the stress with the density. $\rho dl_c = \text{const leads to van Wyk's expression } S \sim (\rho/\rho_0)^3$, while $\rho l_c^2 = \text{const}$ leads to $S \sim (\rho/\rho_0)^2$. Experimental and numerical data provide evidence for the existence of a compaction regime characterized by $S \sim (\rho/\rho_0)^2$ bounded by the van Wyk regime at lower densities and by Toll's regime at higher densities when strong preferential alignment develops. The present work introduces a correction to a well-established structure-properties relation, which is essential in the development of micromechanicsbased constitutive laws for fibrous assemblies. The result has implications for poroelasticity, transport of fluids across networks, and metamaterials whose behavior is modified using prestress.

Acknowledgment

This work was supported in part by the US National Science Foundation (Grant No. CMMI-2022489).

Conflict of Interest

There are no conflicts of interest.

Data Availability Statement

The authors attest that all data for this study are included in the paper.

References

- [1] Picu, C. R., 2022, Network Materials: Structure and Properties, Cambridge University Press, Cambridge.
- [2] Kallmes, O., and Corte, H., 1960, "The Structure of Paper, I. The Statistical Geometry of an Ideal Two Dimensional Fiber Network," Tappi J., 43(9), pp. 737–752.

- [3] van Dillen, T., Onck, P. R., and van der Giessen, E., 2008, "Models for Stiffening in Cross-Linked Biopolymer Networks: A Comparative Study," J. Mech. Phys. Solids, 56(6), pp. 2240–2264.
- [4] Alava, M., and Niskanen, K., 2006, "The Physics of Paper," Rep. Prog. Phys., 69(3), pp. 669–723.
- [5] Dodson, C., 1996, "Fiber Crowding, Fiber Contacts, and Fiber Flocculation," Tappi J., 79(9), pp. 211–216.
- [6] Philipse, A. P., 1996, "The Random Contact Equation and Its Implications for (Colloidal) Rods in Packings, Suspensions, and Anisotropic Powders," Langmuir, 12(5), pp. 1127–1133.
- [7] Toll, S., 1993, "Note: On the Tube Model for Fibre Suspensions," J. Rheol., **37**(1), pp. 123–125.
- [8] Komori, T., and Makishima, K., 1977, "Numbers of Fiber-to-Fiber Contacts in General Fiber Assemblies," Text. Res. J., 47(1), pp. 13–17.
- [9] Yi, Y. B., Berhan, L., and Sastry, A. M., 2004, "Statistical Geometry of Random Fibrous Networks, Revisited: Waviness, Dimensionality, and Percolation," J. Appl. Phys., 96(3), p. 1318.
- [10] Negi, V., and Picu, R. C., 2019, "Mechanical Behavior of Nonwoven Non-Crosslinked Fibrous Mats With Adhesion and Friction," Soft Matter, 15(29), pp. 5951–5964.
- [11] Flory, P. J., 1969, Statistical Mechanics of Chain Molecules, Interscience Publishers.
- [12] Fetters, L. J., Hadjichristidis, N., Lindner, J. S., and Mays, J. W., 1994, "Molecular Weight Dependence of Hydrodynamic and Thermodynamic Properties for Well-Defined Linear Polymers in Solution," J. Phys. Chem. Ref. Data, 23(4), pp. 619–640.
- [13] van Wyk, C. M., 1946, "Note on the Compressibility of Wool," J. Textile Inst., 37(12), pp. T285–T292.
- [14] Toll, S., and Manson, J. A. E., 1995, "Elastic Compression of a Fiber Network," ASME J. Appl. Mech., 62(1), pp. 223–226.
- [15] Toll, S., 1998, "Packing Mechanics of Fiber Reinforcements," Polym. Eng. Sci., 38(8), pp. 1337–1350.
- [16] Schellman, J. A., 1974, "Flexibility of DNA," Biopolymers, 13(1), pp. 217-226.
- [17] Mezeix, L., Bouvet, C., Huez, J., and Poquillon, D., 2009, "Mechanical Behavior of Entangled Fibers and Entangled Cross-Linked Fibers During Compression," J. Mater. Sci., 44(14), pp. 3652–3661.
- [18] Baudequin, M., Ryschenkow, G., and Roux, S., 1999, "Non-Linear Elastic Behavior of Light Fibrous Materials," Eur. Phys. J. B, 12(1), pp. 157–162.
- [19] Alkhagen, M., and Toll, S., 2007, "Micromechanics of a Compressed Fiber Mass," J. Appl. Mech., 74(4), pp. 723–731.
- [20] Baljasov, P. D., 1976, Compression of Textile Fibers in Mass and Technology of Textile Manufacture, Legkaya promyshlennost, Moscow.
- [21] Neckar, B., and Das, D., 2012, Theory of Structure and Mechanics of Fibrous Assemblies, Woodhead Pub, India.
- [22] Abd El-Rahman, A. I., and Tucker, C. L., 2013, "Mechanics of Random Discontinuous Long-Fiber Thermoplastics. Part II: Direct Simulation of Uniaxial Compression," J. Rheol., 57(5), pp. 1463–1489.
- [23] Subramanian, G., and Picu, C. R., 2011, "Mechanics of Three-Dimensional, Nonbonded Random Fiber Networks," Phys. Rev. E, 83(5), p. 056120.
- [24] Barbier, C., Dendievel, R., and Rodney, D., 2009, "Role of Friction in the Mechanics of Nonbonded Fibrous Materials," Phys. Rev. E Stat. Nonlin. Soft Matter. Phys., 80(1), p. 016115.
- [25] Durville, D., 2005, "Numerical Simulation of Entangled Materials Mechanical Properties," J. Mater. Sci., 40(22), pp. 5941–5948.
- [26] Beil, N. B., and Roberts, W. W., 2002, "Modeling and Computer Simulation of the Compressional Behavior of Fiber Assemblies," Text. Res. J., 72(4), pp. 341–351.
- [27] Poquillon, D., Viguier, B., and Andrieu, E, 2005, "Experimental Data About Mechanical Behaviour During Compression Tests for Various Matted Fibres," J. Mater. Sci., 40(22), pp. 5963–5970.